

Use of Inertial Sensors to Support Video Tracking

Michaël Aron, Gilles Simon and Marie-Odile Berger

LORIA - UHP Nancy 1 - INRIA Lorraine

615, rue du Jardin Botanique

54602 Villers-les-Nancy, France

email: {aron,simon,berger}@loria.fr

Abstract

One of the biggest obstacle to building effective augmented reality (AR) systems is the lack of accurate sensors that report the location of the user in an environment during arbitrary long periods of movements. In this paper, we present an effective hybrid approach that integrates inertial and vision based technologies. This work is motivated by the need to explicitly take into account the relatively poor accuracy of inertial sensors and thus to define an efficient strategy for the collaborative process between the vision based system and the sensor. The contributions of this papers are threefold: (i) our collaborative strategy fully integrates the sensitivity error of the sensor : the sensitivity is practically studied and is propagated into the collaborative process, especially in the

matching stage (ii) we propose an original online synchronization process between the vision based system and the sensor. This process allows us to use the sensor only when needed. (iii) an effective AR system using this hybrid tracking is demonstrated through an e-commerce application in unprepared environments.

Keywords: Augmented reality, camera tracking, sensor fusion

1 Introduction

Augmented reality systems supplement the real world with virtual (computer generated) objects that appear to coexist seamlessly in the same space as the real world. Potential applications of AR are important and include maintenance and repair of complex equipments, medical visualization, collaborative work, and applications in cultural heritage [1]. Though promising, AR is barely at the demonstration phase today and several challenges must be overcome to prove the full potential of AR. Despite remarkable progress in the field in the late 1990s, there are still major obstacles limiting the wider use of AR both for technological limitations and because of insufficient robustness and accuracy of the tracking stage in practical situations. The term tracking is used here to describe real time pose recovery from monocular video streams.

The tracking task is difficult because registration must be achieved sequentially at video rate, with a high accuracy and a good repeatability during arbitrary long periods of movements. This means that the accuracy of the pose should be the same at the beginning of

the applications and at the end of the process. Systems that provide accurate and repeatable registration are of interest because they would make possible new applications areas that cannot be handled by existing AR systems.

Whatever the technology used for tracking, most AR systems require carefully controlled environments or restrict the motion of the user to ensure robustness of the registration stage over time:

- Inertial tracking are a popular choice due to their high frequency response and their independence from external beacons. However, they lack long term stability due to sensor noise and drift. Their accuracy is generally poor (in the range $[\cdot 25, 1]$ degree)
- Magnetic and ultrasound sensors have been used successfully but confine the user to an instrumented and small working volume.
- Vision-based methods are generally more accurate as they depend on features that are directly extracted from the images to be augmented. However, their robustness is tightly related to the efficiency of feature extraction/tracking through the sequence. They cannot generally keep up with quick or abrupt motion because the 2D tracking may fail in these conditions.

Using a single modality then leads AR systems to restrict or to constraint the movements of the user and prevents the user to walk and look anywhere he pleases. The idea to make collaborate two technologies in order that the sensor complementarity nature helps

overcome camera/sensor specific deficiencies is not new and was pioneered by [2] for autonomous navigation of a mobile robot. In AR, researches started with State in 1996 [3], followed by [4, 5]. In most applications, the strategy to combine the sensors is the same for every frame: the inertial or gyro data are used to predict feature positions and to make easier feature detection and tracking [6, 5]. A Kalman filter is then often used to reduce drift and to fuse the data [7]. Unfortunately, Kalman filters require a kinematic model of the sensor. This model is usually based on the hypothesis of regular motion (as constant acceleration) and are thus unable to take into account non-systematic events as abrupt head motions. To overcome this problem, we took a different approach and decided to use the inertial sensor only when needed, that is when we detect that the vision based system does not give reliable results. This approach has some ideas in common with [8] in the context of mobile robots guided by odometry and gyro sensors: localization is always based on odometry and the authors switch to a gyroscope only when catastrophic failures occur.

Our method rests on the same strategy and we here proposed a method which only uses the inertial sensor when the confidence in the vision based system is limited. The contributions of this paper with respect to existing approaches in the field are the following:

- We do not attempt to fuse the data. The sensor data are here used to guide or to re-initialize the matching stage. This avoids to put constraints on the user's motion.
- We propose an efficient mean to detect when the confidence in the vision based system is not sufficient and must be supplemented by the sensor data.

- We do not attempt to update and to correct the drift of the sensor. Relative sensor data are only used between two image acquisitions. Hence ill-effects of drift are less important.
- Hybrid systems require synchronization among different sensors. Synchronization is of special importance for high motion rate because synchronization delay will cause large error in image prediction and the system will likely fail. The synchronization problem is seldom addressed in AR though it is very difficult to achieve in practice as noted in [5]. One of the contribution of the paper is to prove that the synchronization delay between camera and sensor is generally not constant over time and we propose an efficient solution to evaluate this delay on line.

The efficiency of our hybrid system is demonstrated on our plane based AR system [9] associated with the inertial sensor MT9 (Xsens). It must be noted that our method is suited to any camera tracking system based on the following framework: 1. Poses are obtained from feature correspondences tracked over consecutive frames. 2. A numeric criterion which enables to judge if the pose is computed with sufficient reliability must be available. A typical example of such a criterion is the number of features that have been correctly tracked in the current frame (inlier features). This information is generally obtained by introducing M-estimators or the RANSAC paradigm in the pose computation algorithm. Many systems can be found in the literature that implement this architecture [10, 11].

The paper is organized as follows: the accuracy of the inertial sensor is assessed in

section 2. Camera/sensor collaboration is extensively described in section 3 and section 4 is devoted to our original algorithm for on-line sensor/camera synchronization. The complete system developed within the European ARIS project as well as results are demonstrated in section 5 and 6.

2 Sensor accuracy

Inertial sensors are three-degree of freedom orientation trackers that combine accelerometers and magnetometers to compensate for otherwise unlimited increasing errors from the integration of rate of turn data (gyroscopes). Recent advances in the miniaturization of all these components made it possible to integrate them in very small boxes (typically $39 \times 54 \times 28$ mm), distributed at reasonable rates (example manufacturers are Xsens and InterSense). As they are based on natural physical phenomenon and do not require any special instrumentation of the environment, they are well suited to outdoor AR. However, technical specifications given by manufacturers indicate a $< 1^\circ$ RMS accuracy for the most recent products, which is unfortunately still insufficient to obtain convincing augmented scenes.

In this section, we present accuracy tests we performed on a particular inertial sensor (the Xsens MT9-B), in order to assess the accuracy of this kind of sensors, and check if a Gaussian distribution is well suited to describe the errors we obtain on the provided Euler angles. In these experiments, the sensor was fixed on a computer controlled pan-tilt unit (PTU), whose resolution was 0.013° . Three sets of tests were performed, changing for each

set the alignment between the sensor and the PTU axes (two configurations are presented in Fig. 1).

For each configuration, rotation commands of different amplitudes (2, 5, 10, 15 and 20 degrees) were individually sent to each axis of the PTU (1000 rotations per amplitude and per axis). Means and standard deviations of the values provided by the sensor and histograms of the centered values are shown in figure 1. As the sensor and PTU axes were not perfectly aligned, the means we obtain for each amplitude are not exactly equal to the requested amplitudes. However, two major information can be inferred from these results: 1. the accuracy of the angles provided by the sensor does not significantly depend on the amplitude of the rotation and 2. the accuracy of the angles obtained around a particular axis of the sensor depends on the initial orientation of this axis with regard to the PTU. For example, angles around x -axis are much more accurate in configuration 1 than in configuration 2. Actually, the vertical axis (with regard to the earth) of the sensor always provides less accurate results than the horizontal axis. This is due to the fact that magnetometers that compensate the gyroscopes drift around the vertical axis are less accurate than accelerometers that compensate the drift around non vertical axes. Indeed, magnetometers are sensitive to ferromagnetic perturbations of the environment, whereas accelerometers are based on the gravitational axis which is more reliable.

In practical situations, the sensor is fixed horizontally on the camera, so that the z -axis is initially up. In this situation, we expect a 3D Gaussian noise whose mean is null and standard deviations deduced from our sets of tests (namely, $\sigma_z = 0.499^\circ$ and $\sigma_x = \sigma_y = 0.155^\circ$).

During the tracking process, standard deviations are interpolated online according to the angles between the related axes and the z -axis of the sensor in its initial orientation.

3 Camera-sensor collaboration

3.1 Hand-eye calibration

Integrating sensor data in vision-based camera tracking first requires that the alignment between the sensor and the camera is known. Formally, this consists of finding a rotation matrix X that permits to deduce camera rotations B from sensor rotations A (Fig. 2), according to the following equation:

$$AX = XB \tag{1}$$

The hand-eye calibration task consists of determining matrix X from this equation, applied to several pairs of matrices A and B (three at minimum), obtained from different orientations of the camera-sensor device. Many methods have been proposed to solve the generated set of equations. In this work we use the method proposed by Park and Martin [12].

3.2 Integration strategy

Our strategy for integrating sensor data in vision-based tracking rests on the fact that the vision based system gives accurate position estimation [3] except when non-systematic events such as head motions occur. The sensor is then used to provide the vision system with a

fair prediction of the tracked features despite the occurrence of abrupt motions. Hence we do not fuse sensor and vision data. Sensor data are only used to guide and to reinitialize the vision process

We do not make a systematic use of the sensor data because their relatively poor accuracy may lead to incorrect pose estimation. The following example illustrates that point: the 99% confidence limit of the sensor angle distribution error observed in section 2 for the z -axis is equal to $2.58 \times \sigma_z = 1.29^\circ$. This corresponds to an horizontal image error of 23 pixels (at the principal point) for a typical focal length of 1024 pixels. This may have different consequences, depending on how the sensor is used: if sensor data are used systematically to provide the rotational part of the camera motions, this will induce very inaccurate and jittering augmentations; if sensor data are used systematically to predict the position of the features from their positions in the previous image, tracking will fail in 1% of the cases for a typical 20 pixels half-size research window, that is every five seconds in mean for a 20 fps process.

Another reason for the non systematic use of the sensor is the need to synchronize sensor and vision acquisition to perform hybrid estimation. As noticed in [5], accurate synchronization is needed especially when large motion may occur in the sequence. Indeed, approximate synchronization may lead to associate a large motion predicted by the sensor to a wrong image, making the system fail. However, experiments reported in section 4 proved that the synchronization delay is not constant over time and must be estimated online, inducing additional processing time: the computation time of the vision based camera tracking depends

on characteristics of each frames, and this variable time needs to be synchronized with data acquisitions of the inertial sensor. Hence, due to real-time constraints, non-systematic use of the sensor appear as the most appropriate cooperation framework between vision and sensor.

3.3 Sensor-based feature prediction

This paragraph explains how to integrate inertial sensor data to guide the feature tracking process, after an abrupt camera rotation occurred (which corresponds to the common case of rapid head motions). However, the results presented below can most of the time be adapted to any kind of motion, providing that the appropriate sensor is used and its accuracy quantified.

When a camera rotation occurs, the whole image is transformed according to a 3×3 matrix H called *homography*, given by [13]:

$$H = KBK^{-1}, \quad (2)$$

where K is the camera intrinsic parameters matrix and B the rotation matrix. This means that a pixel at position m in the previous frame appears at position $m' = Hm$ in the new frame (m and m' are homogeneous coordinate vectors).

Therefore, combining equations (1) and (2) yields a function p which, assuming a sensor rotation matrix A is known, provides a prediction of the new position of any pixel m at

coordinates:

$$p(m) = KX^t AXK^{-1}m. \quad (3)$$

3.4 Error propagation

In addition of these predicted feature positions, our method provides optimal research regions. These regions are confidence ellipses that are obtained by propagating sensor errors during the calibration and acquisition processes.

Sensor error analysis yields a covariance matrix of the provided parameters: for the inertial sensor, we get a covariance matrix of the Euler angles $\alpha_A, \beta_A, \gamma_A$:

$$\Sigma_A = \begin{pmatrix} \sigma_z^2 & 0 & 0 \\ 0 & \sigma_y^2 & 0 \\ 0 & 0 & \sigma_x^2 \end{pmatrix},$$

(inter-axes covariances have proven negligible in our experiments). This matrix is used to recover the covariance matrix Σ_X using error propagation from the hand-eye equation (computation details are given in appendix). For a predicted position $m' = p(m)$, we can therefore compute a covariance matrix $\Sigma_{m'}$ using the following linear approximation:

$$\Sigma_{m'} = J_{X/m}\Sigma_X J_{X/m}^t + J_{A/m}\Sigma_A J_{A/m}^t,$$

where

$$J_{A/m} = \left(\frac{\partial p}{\partial \alpha_A} \quad \frac{\partial p}{\partial \beta_A} \quad \frac{\partial p}{\partial \gamma_A} \right),$$

$$J_{X/m} = \left(\frac{\partial p}{\partial \alpha_X} \quad \frac{\partial p}{\partial \beta_X} \quad \frac{\partial p}{\partial \gamma_X} \right)$$

(camera intrinsic parameters are supposed exact and computed before the AR application).

This provides a confidence ellipse around m' , defined by equation

$$X^t \Sigma_{m'}^{-1} X \leq 9.21, \quad (4)$$

9.21 being the 99% confidence limit for a two degrees of freedom chi-square.

4 Online synchronization

To check and determine the synchronization delay between these two devices, we first implemented a procedure based on abrupt motion detection. Several abrupt motions were performed in a same shoot of a scene that allows easy detection of visual motions (Fig. 5.b). Abrupt changes in rotation angles were matched to abrupt changes in image intensities distribution (a criterion is proposed by Prager in [14] in the context of the temporal calibration of a freehand ultrasound probe). These experiments made obvious that the synchronization delay between the two devices is not constant over time (see Fig. 3, where three successive abrupt motions were applied in a same shoot and lead to non constant acquisition delay). This means that synchronization of the two devices must be performed online.

In our set-up, sensor data are always available before image data. Indeed, the time needed to capture a video frame (here referred to as *acquisition cycle*) is large compared to the time needed to sample information from the inertial sensor. For each acquisition cycle, the relative sensor data acquired during the cycle are composed and allow us to compute the *sensor homography*, that is the homography computed from the sensor during an acquisition

cycle. These homographies will be used to guide feature tracking when the vision-based system fails.

The underlying ideas of our algorithm are explained on a synthetic example (Fig. 4). Three main steps are needed to perform on line synchronization:

Identification of the vision based system failure

A decrease in the number of inliers (i.e number of points successfully matched by the system) is a good mean to detect that the vision system is going to fail. Non successful matching is generally due to the fact that the corresponding point is outside the research window and is thus not detected by the system. The number of inliers is especially relevant for planar-based system because tracking planar structures can be made very robust due to homographic constraints [13]. In our example, this number decreases drastically in frame 11, which means that sensor information is required in that frame.

Identification of the corresponding sensor data

Once a tracking failure has been detected, the corresponding sensor homography has to be identified. The principle of our method is to simulate the propagation of the features obtained just before failure, using each buffered sensor homography, and choose the one that makes the matching process fail.

In the visual system, matching fails when the researched feature lies outside the research region. Hence, the corresponding sensor data will also give rise to a predicted point that is

outside the research window. Our procedure amounts to choose the homography that makes the number of *sensor-predicted inliers* (features that are propagated inside the research region) decrease dramatically. In our example, this allows us to identify at buffer position 3 the inertial data that correspond to the visual tracking failure. It must be noted that another possibility for sensor data identification may consist in detecting abrupt variations in the acquired angles. Unfortunately, this criterion is not relevant as the effect of angles variations on the images also depends on the depth of the scene and on the camera position with respect to the scene. As a result, some abrupt motion of the camera can be perfectly handled by the vision-based system while others cannot be handled.

Use of the inertial data to re-initialize the matching stage

Once the corresponding sensor homography has been identified at position p in the storing buffer, inertial data can be used to re-initialize the matching stage. To this aim, homographies in the buffer are considered from position p , and the matching process is tried using the accumulated homography. Accumulating homographies is necessary as a rapid rotation may last more than one acquisition cycle.

5 ARIS tracking system

The goal of the ARIS project was to provide new and innovative AR-technologies for e-(motion)-commerce application, where the products can be presented in the context of their

future environment. A mobile AR-unit was developed, where 3D product models (e.g. furniture) can be directly visualized on a real site, taking consistent geometry and illumination of real and virtual objects into account. The user can check the aesthetic result and the actual fit of the furniture item into the room, and also discuss with remote participants, taking shared augmented technologies into account. This section describes parts of the system that concern pose computation and interaction with the environment. Results of the complete tracker obtained on a real-world scene are shown in figure 5. A complete video (called VIDEO1) is provided on our web site¹.

Camera tracking

Our collaborative tracking system is based on the vision-based method we proposed in [9]: key-points belonging to planar surfaces are tracked in consecutive images, providing homographies that enable to update the pose (assuming the equations of the planes are known). False matches are identified using the RANSAC paradigm (Fig. 5.(a)), and sensor data are incorporated according to the method presented in this paper. This results in a robust system where the user is able to move with increased freedom. Tracking is performed at 15 fps on a classical laptop and web-cam configuration. The hand-eye calibration is performed by shooting a calibration target from different views. Markers are placed on the target in order to automate the calibration process (Fig. 5.(b)).

¹<http://www.loria.fr/equipes/magrite/movies/cavw.html>

Reconstruction of the scene geometry

The geometry of the scene is needed both for tracking and for handling photometric and geometric interactions between real and virtual objects. This geometry is acquired offline from a single image of the scene with the help of an interactive reconstruction tool. Intrinsic parameters and the initial camera pose are recovered from a poster laid in a corner of the room (Fig. 5.(c)).

Interaction with the environment

As camera poses are computed with respect to a world reference frame, synthetic objects can be added in the real scene at any time of the tracking process (Fig. 5.(d-f)). These objects can easily be placed in the real scene by sliding them on the recovered structure, mutual occlusions and collisions between real and virtual objects being automatically handled.

6 Results

6.1 Synthetic data

In order to assess the relevance of using confidence ellipses instead of rectangle research windows, we simulated thousands of hand-eye calibrations and camera / sensor rotations, adding a Gaussian noise to sensor data (standard deviations were taken as explained in section 2). A relevant research region is a region that maximizes the probability $P(inlier)$ of getting the researched corresponding feature inside the region, while minimizing the

number of non corresponding features $\#outliers$ included in that region. These values were computed using rectangle research regions of different sizes and ellipses corresponding to different confidence limits in equation (4). Figure 6 gives the evolution of $\#outliers$ in function of $P(inlier)$, for different numbers of point features n , randomly chosen inside a 512×512 frame: the curve corresponding to elliptic regions is generally significantly below the curve corresponding to squared regions. For example, a typical 20 pixels half-size research window yields to a mean number of 12 outliers for 2000 points in a 512×512 image. Using elliptic research regions with the same value of $P(inlier)$ reduces the number of expected outliers to 9 (25% less). This reduction is significant as it decreases the risk of ambiguity as well and the computation time needed for the matching process.

6.2 Real sequences

Figure 7.(a) shows the number of inlier correspondences we obtained in a miniature scene sequence (see VIDEOS2 on our web site). Video tracking-less periods are indicated using dashed bars. They correspond to abrupt motions that are all well handled using sensor information. The numbers of sensor-predicted inliers computed using the buffered sensor homographies at frame 173 are shown in figure 7.(b). This illustrates the relevance of using this criterion for online synchronization (a fall is clearly observed at position 1) instead of the sensor rotation amplitude criterion which is less discriminant (Fig. 7.(c)).

Tracking was also performed on real-size scenes (see our web site, VIDEOS 3 and 4).

The first one was shot in the basement of our laboratory (Fig. 8). A user made free motions inside the room, and virtual furnishings were added online. Ten abrupt motions were detected and well handled during this process. The second sequence concerns an outdoor scene that was shot from a camera put on a tripod (Fig. 9) : in that configuration, the whole image is transformed according to a homography. Sensor information was successfully used at thirteen moments of that sequence.

7 Conclusion

We presented a hybrid approach for AR registration with integrated inertial and vision technologies. The complete AR system was successfully demonstrated in unprepared multi-planar environments. Our framework brings significant improvements to the AR system by increasing the freedom of the user during the application. Furthermore, our AR system requires no specific or expensive hardware and can be used with an ordinary laptop and a simple webcam.

Unlike existing approaches, we do not attempt to perform fusion of the two technologies at each frame of the sequence. On the contrary, we restrict the use of each sensor for situations where its contribution is relevant. As a result, we use sensor information only when needed, that is when the pure vision-based system fails to track the camera. In addition, sensor errors are measured and taken into account in the feature matching process. Finally, we address the camera/sensor synchronization problem and propose a method to

resynchronize these two devices online.

There are several improvements and extensions that can be made to our approach. First, the use of an inertial sensor only allows us to consider abrupt rotational motions, as head motions. If more general motions including a large translation part have to be considered, our method can be extended to the use of a position sensor. Second, extensions of the method should concern the vision based system. For numerous pose algorithms as ours, the pose computation process is incremental and may progressively diverge because of successive approximations. Markers, natural features or key-views in the scene could be used to detect system divergences and reinitialize the tracking when necessary.

Appendix: Error propagation in hand-eye calibration

Hand-eye matrix X is solution of the set of equations

$$A_i X = X B_i, \tag{5}$$

where (A_i, B_i) are n sensor/camera rotation pairs. Our aim is to compute a covariance matrix Σ_X of the Euler angles $\alpha_X, \beta_X, \gamma_X$ of matrix X , considering that camera rotations B_i are certain but sensor rotations A_i uncertain.

Equations (5) can be written as $f(x, a) = 0$, where x is a vector of size 3 containing the Euler angles of rotation X , a is a vector of size $3n$ containing the Euler angles of rotations

A_i , and $\mathbf{0}$ is a $9n$ null vector. A first order approximation of $f(x, a)$ gives:

$$f(\bar{x}, \bar{a}) + \frac{\partial f}{\partial x}(\bar{x}, \bar{a}) (x - \bar{x}) + \frac{\partial f}{\partial a}(\bar{x}, \bar{a}) (a - \bar{a}) \approx 0,$$

where \bar{a} and \bar{x} are the estimated values of a and x . This leads to:

$$C \Sigma_X C^t = D [\Sigma_A] D^t,$$

where $C = \frac{\partial f}{\partial x}(\bar{x}, \bar{a})$, $D = \frac{\partial f}{\partial a}(\bar{x}, \bar{a})$ and $[\Sigma_A]$ is the $3n \times 3n$ matrix $\begin{pmatrix} \Sigma_A & & 0 \\ & \Sigma_A & \\ & & \dots \\ 0 & & \Sigma_A \end{pmatrix}$.

Therefore, Σ_X can be expressed as:

$$\Sigma_X = (C^t C)^{-1} C^t D [\Sigma_A] D^t C (C^t C)^{-1}.$$

Acknowledgment

We would like to acknowledge the European Union for funding this work, as part of the ARIS project (IST-2000-28707).

References

- [1] R. T. Azuma, Y. Baillet, R. Behringer, S. Feiner, S. Julier, and B. MacIntyre. Recent Advances in Augmented Reality. *IEEE Computer Graphics and Applications*, pages 34–47, December 2001.
- [2] T. Vieville, F. Romann, B. Hotz, Herve Mathieu, Michel Buffa, Luc Robert, P. Fa-cao, Olivier Faugeras, and J.T. Audren. Autonomous navigation of a mobile robot

- using inertial and visual cues. In *Proceedings of the IEEE International Conference on Intelligent Robots and Systems*, 1993.
- [3] A. State, G. Hirota, D. Chen, W. Garrett, and M. Livingston. Superior Augmented Reality Registration by Integrating Landmark Tracking and Magnetic Tracking. In *Computer Graphics (Proceedings Siggraph New Orleans)*, pages 429–438, 1996.
- [4] K. Satoh, M. Anabuki, H. Yamamoto, and H. Tamura. A hybrid registration method for outdoor augmented reality. In *International Symposium on Augmented Reality, Los Alamitos*, pages 67–76, 2001.
- [5] B. Jiang, S. You, and U. Neumann. A robust hybrid tracking system for outdoor augmented reality. In *IEEE Virtual Reality 2004, Chicago*, pages 3–10, March 2004.
- [6] G. Klein and T. Drummond. Tightly Integrated Sensor Fusion for Robust Vision Tracking. In *Proceedings of the British Machine Vision Conference, Cardiff*, pages 787–796, September 2002.
- [7] Eric Foxlin and Leonid Naimark. Vis-tracker: A wearable vision-inertial self-tracker. In *IEEE Virtual Reality 2003 (VR2003), Los Angeles, CA*, March 2003.
- [8] J. Borenstein and L. Feng. Gyrodometry: A New Method for Combining Data from Gyros and Odometry in Mobile Robots. In *IEEE ICRA, Minneapolis, Minnesota*, pages 423–428, 1996.

- [9] G. Simon and M.-O. Berger. Pose estimation for planar structures. *IEEE Computer Graphics and Applications, special issue on Tracking*, pages 46–53, nov 2002.
- [10] C.J. Harris. Tracking with Rigid Models. In *Active Vision*, chapter 4. Blake and Yuille, MIT Press, 1992.
- [11] K. W. Chia, A. D. Cheok, and S. J. D. Prince. Online 6 DOF Augmented Reality Registration from Natural Features. In *Proceedings of International Symposium on Mixed and Augmented Reality, Darmstadt, Germany*, pages 305–313, 2002.
- [12] F. Park and B. Martin. Robot Sensor Calibration: Solving $AX=XB$ on the Euclidean Group. *IEEE Transactions on Robotics and Automation*, 5(10):717–721, 1994.
- [13] R. I. Hartley and A. Zisserman. *Multiple View Geometry in Computer Vision*. Cambridge University Press, ISBN: 0521623049, 2000.
- [14] R. W. Prager, A. H. Gee, and L. Berman. Stradx: real-time acquisition and visualisation of freehand 3D ultrasound. report `cued/f-infeng/tr 319`, Cambridge University Department of Engineering, 1998.

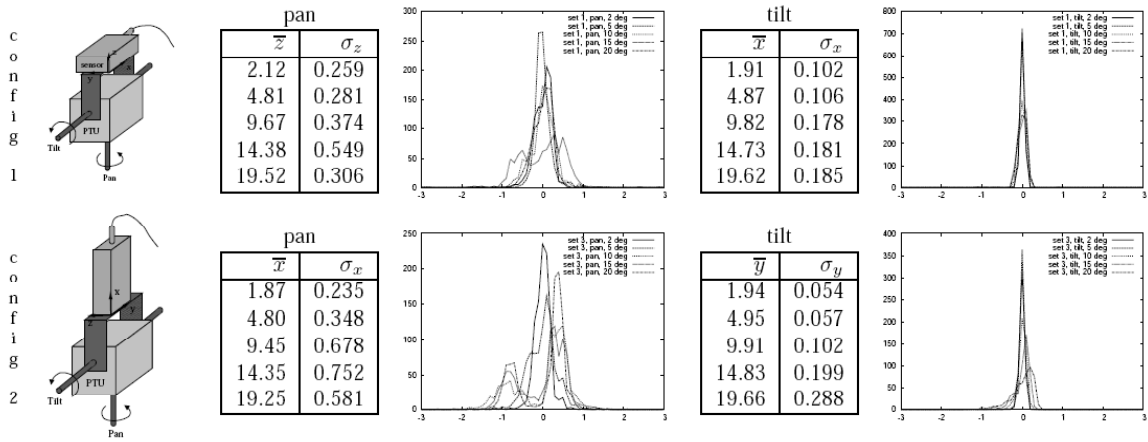


Figure 1: Precision results obtained over the three axes of the Xsens MT9-B inertial sensor according to its absolute orientation.

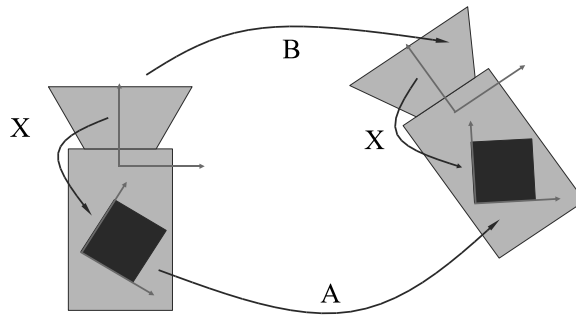


Figure 2: Hand-eye transformation.

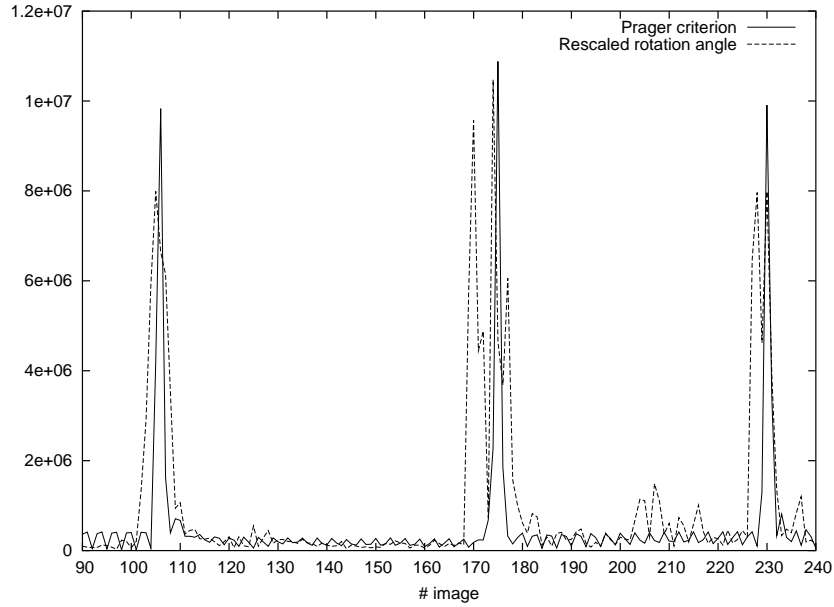


Figure 3: The synchronization delay between the inertial sensor and the camera is not constant over time. Peaks in bold line correspond to abrupt changes in the images and peaks in dotted lines are for abrupt changes in the inertial data. The delays between image and sensor acquisition are not constant over time and are successively equals to 1, 5 and 2 images.

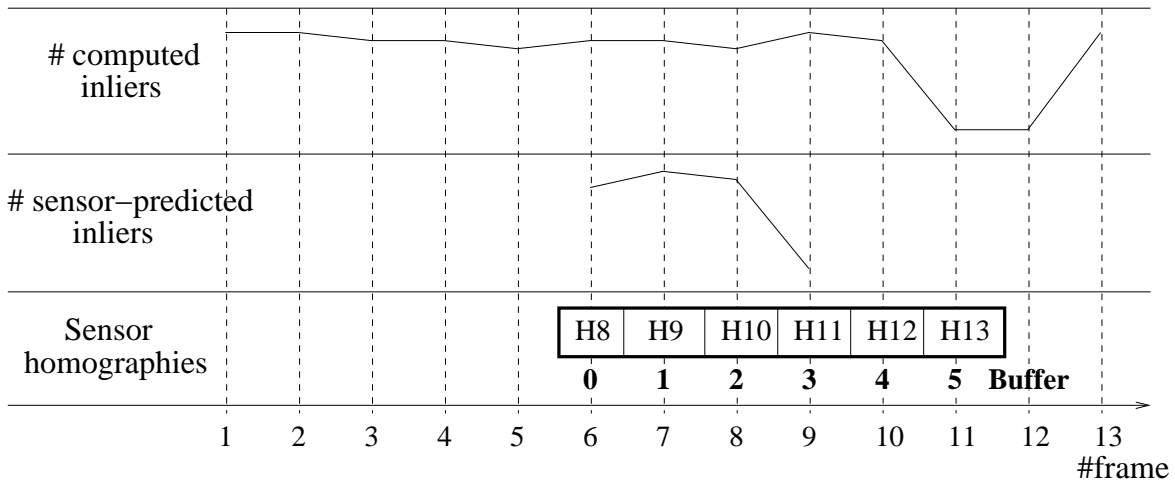


Figure 4: Online synchronization between camera and sensor.



(a)

(b)



(c)

(d)



(e)

(f)

Figure 5: Tracking and interaction in the ARIS system. (a) Camera tracking: green segments join the corresponding key-points between the current and the previous frame. Red segments are used to show outlier correspondences. (b) The hand-eye calibration is performed using markers on a box. (c) Camera parameters and scene geometry are obtained using geometric constraints from a single image. (d-f) Virtual objects are placed with regard to the recovered structure of the scene, which enables online visualization and interaction.

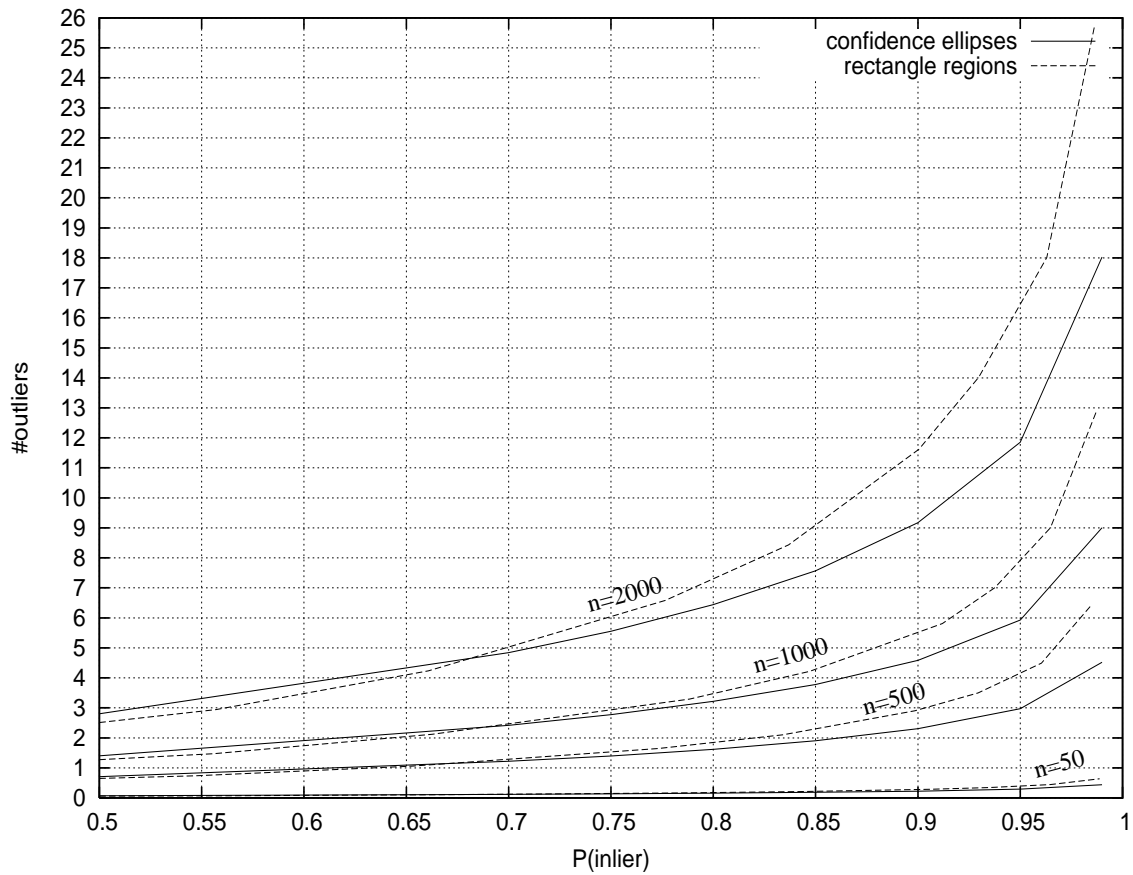
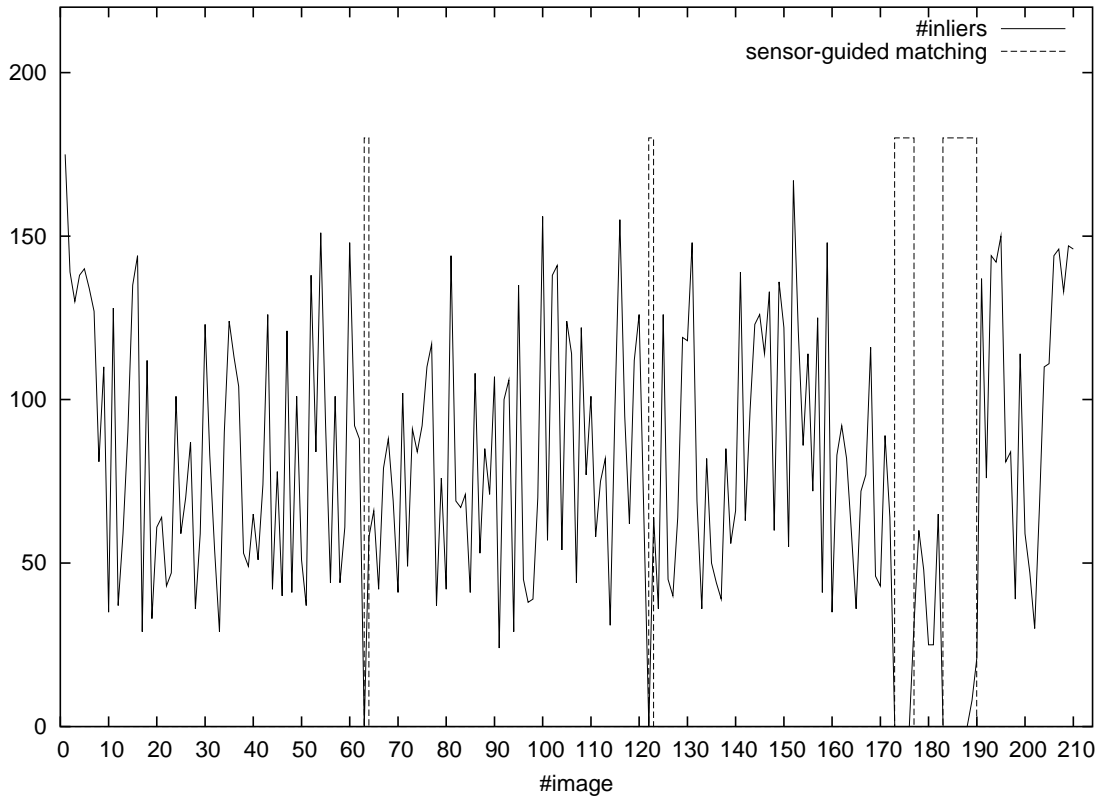
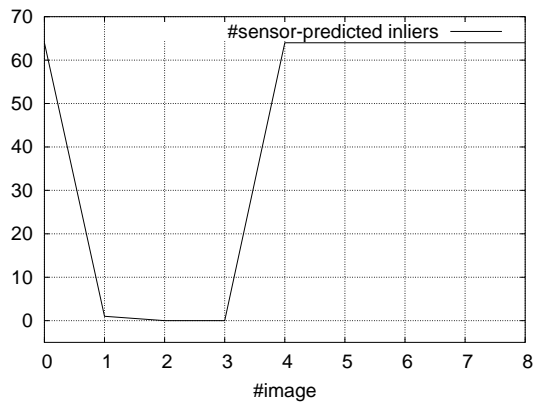


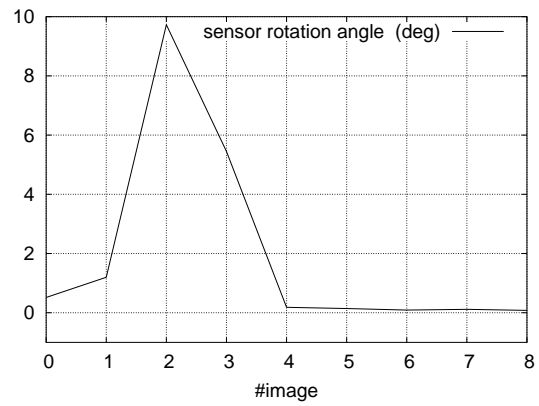
Figure 6: The expected number of outliers in function of the probability of getting the inlier inside an elliptic or rectangular research region, for different number of points.



(a)



(b)



(c)

Figure 7: (a) Number of inlier correspondences and tracking-less periods obtained in a miniature scene sequence. (b),(c) Comparison of two synchronization criteria at frame 173 of that sequence.



Figure 8: Example results obtained at two instants of an indoor sequence. Top: augmented frames before an abrupt motion occurred. Middle: correspondences obtained by using sensor predictions (white segments are inlier correspondences, black segment are outliers identified by RANSAC). Bottom: augmented scenes after the abrupt motion occurred.

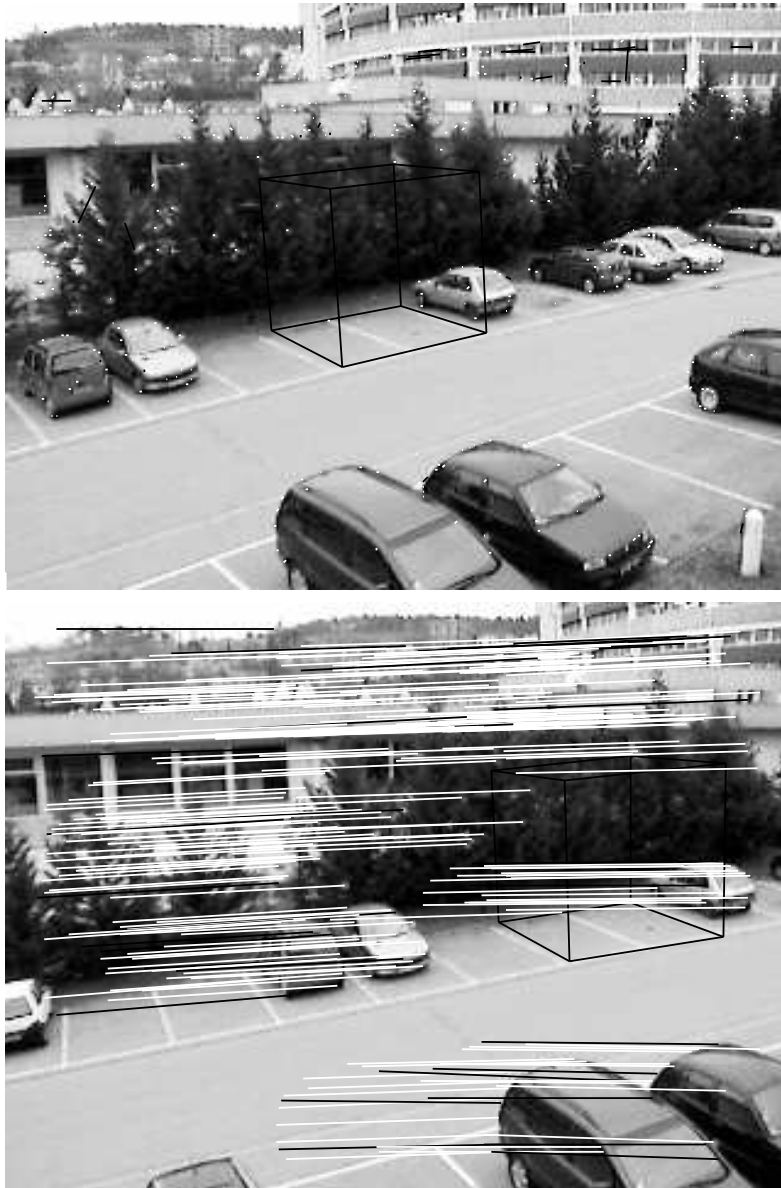


Figure 9: A sensor-guided tracking result obtained in an outdoor sequence. Top: frame 486 with a virtual cube added. Bottom: frame 488 and the recovered correspondences.